Journal of Electron Spectroscopy and Related Phenomena 199 (2015) 19–26

Contents lists available at ScienceDirect

Journal of Electron Spectroscopy and Related Phenomena

journal homepage: www.elsevier.com/locate/elspec

What is the correct Fe L_{23} X-ray absorption spectrum of magnetite?

Xiaohui Zhu [a], Samanbir S. Kalirai [a,1], Adam P. Hitchcock [a,*], Dennis A. Bazylinski [b]

[a] Department of Chemistry and Chemical Biology, McMaster University, Hamilton, ON L8S 4M1, Canada
[b] School of Life Sciences, University of Nevada at Las Vegas, Las Vegas, NV 89154-4004, USA

ARTICLE INFO

Article history:
Received 1 September 2014
Received in revised form 3 December 2014
Accepted 11 December 2014
Available online 5 January 2015

Keywords:
Magnetite
Maghemite
Fe L_{23} spectra
XMCD
MV-1 magnetotactic bacteria
Nano-magnetite

ABSTRACT

Various groups have reported Fe L_{23} X-ray absorption spectra (XAS) of magnetite (Fe_3O_4), each claiming to be that of magnetite, but which contradict each other. Here we report an XAS study of two kinds of magnetite: one is biogenic magnetite nanocrystals extracted from the magnetotactic bacterium *Magnetovibrio blakemorei* strain MV-1; the other is synthetic, abiogenically produced nano-magnetite. We see significantly different XAS spectra of these two materials. Only when the abiogenic magnetite was reduced under H_2 did it give the same spectrum as the biogenic sample. Extensive heating of the biogenic magnetite in air produced spectra similar to that of the abiogenic magnetite. These two spectra are typical of the range of published Fe L_{23} spectra of magnetite. X-ray diffraction confirmed that the biogenic material is stoichiometric Fe_3O_4, and showed that the as-received or partly reduced abiogenic material is a non-stoichiometric oxide, intermediate between magnetite and maghemite (γ-Fe_2O_3). When the membrane which surrounds magnetosome chains was intact, the biotic magnetite single crystals were surprisingly resistant to oxidation. This study clarifies a significant confusion existing in the literature as to the correct Fe L_{23} X-ray absorption spectra of magnetite and maghemite.

1. Introduction

Iron oxides, a group of minerals consisting of iron and oxygen and/or hydroxide, include some of the most important transition metal oxides [1]. To date, there are sixteen known phases of iron oxides differing in composition, Fe valence, and crystal structure [2]. Among them, magnetite (Fe_3O_4) and maghemite (γ-Fe_2O_3) are two particularly important members based on their unusual properties. For example, they are the only magnetic materials approved for use in biomedical applications [3,4]. They are also used in magnetic storage media [5], gas sensing materials [6], as catalysts [7], and they are being evaluated as electrodes in Li-ion batteries [8]. Fe_3O_4 and γ-Fe_2O_3 are of strong fundamental interest due to their interesting physical and chemical properties. Fe_3O_4 has an inverse spinel structure with space group Fd3 m and a unit cell edge length of 8.3941 Å [9]. It is a mixed valence compound with a Fe(II)/Fe(III) ratio of 0.5. In each unit cell, the tetrahedral sites are occupied by 8 Fe(II) ions while the octahedral sites are occupied by a random distribution of 8 Fe(II) and 8 Fe(III) ions. γ-Fe_2O_3 is iso-structural with Fe_3O_4 but has a slightly smaller lattice constant of 8.3474 Å [2]. It has no divalent Fe ions and the trivalent Fe ions are positioned in the tetrahedral and octahedral sites.

Due to the structural similarities between Fe_3O_4 and γ-Fe_2O_3, it is difficult to distinguish these two oxides. The Fe 2p photoelectron spectra of these two species are very similar but distinguishable [10]. Acidic dissolution, Mössbauer spectroscopy and powder X-ray diffraction are common approaches to address the issue of stoichiometry in magnetite [11–13] but they all have limitations [14]. The acidic dissolution method cannot be applied to natural or mixed-phase samples which contain other redox active components or functional groups. Mössbauer spectroscopy and powder X-ray diffraction are limited by the effect of impurities which could influence results obtained by these two methods. Thus, additional methods are required for characterizing magnetite samples, particularly for nanoparticle samples.

Over the past two decades, synchrotron-based soft X-ray spectroscopy and imaging techniques, in particular X-ray absorption spectroscopy (XAS) with circularly polarized light, have been used to measure electronic properties of samples, through the near edge structure, and magnetic properties, through the X-ray magnetic circular dichroism (XMCD) signal. XAS is a suitable technique since the near edge fine structure is an excellent probe of valence state, local bonding and structure, while XMCD provides element and crystal site-specific magnetic moments of transition-metal ions [15–17]. Many different groups have reported X-ray absorption spectra of materials which are claimed to be magnetite (Fe_3O_4

* Corresponding author. Tel.: +1 905 525 9140x24749; fax: +1 905 521 2773.
E-mail address: aph@mcmaster.ca (A.P. Hitchcock).
[1] Present address: Inorganic Chemistry and Catalysis, Utrecht University, 99 Universiteitweg, Utrecht, The Netherlands.

http://dx.doi.org/10.1016/j.elspec.2014.12.005
0368-2048/

Table 1
Summary of published L-edge XAS spectra of Fe_3O_4 and γ-Fe_2O_3.

Sample	Synthetic method	Shoulder at 708 eV (Y/N)	Detection method	Reference
Fe_3O_4 thin film	Epitaxy on MgO	Partly	TEY	[18]
Fe_3O_4 ultrathin film	Epitaxy on Pt (1 1 1)	N	TEY	[19]
Fe_3O_4 colloid	Co-precipitation	Y	TEY	[20]
Fe_3O_4	Unspecified	Y	TEY	[21]
Fe_3O_4 nanoparticles	Reacting iron salts in microemulsion reactors	N	TEY	[22]
Fe_3O_4 thin film	Pulsed laser deposition	N	TEY	[23]
Fe_3O_4 single-crystalline sample	–	N	TEY	[24,25]
Fe_3O_4 nanoparticles	Solution based	Y	TEY	[26]
Fe_3O_4 nanoparticles	From Alfa Aesar	Y	Transmission	[27]
Fe_3O_4 nanoparticles	Solution based	Y	TEY	[28]
Fe_3O_4 film	Epitaxy on GaAs (0 0 1)	N	TEY	[29]
γ-Fe_2O_3 film	Oxygen-plasma-assisted molecular beam epitaxy	N	TEY	[30]
γ-Fe_2O_3 nanoparticles	Solution based	N	TEY	[31]
γ-Fe_2O_3 nanoparticles	Soft chemistry in a two-step process	N	TEY	[32]
γ-Fe_2O_3 nanoparticles	Sono-chemistry	Y	TEY	[33]
γ-Fe_2O_3 nanoparticles	Solution based	Y	TEY/TFY	[34]
γ-Fe_2O_3 nanoparticles	Solution based	Y	TEY	[35]
γ-Fe_2O_3 nanoparticles	Biomineralized by *Helicobacter pylori*	Y	TEY	[36]
γ-Fe_2O_3 nanoparticles	Wet synthesis method	Y	TEY	[37]

TEY, total electron yield; TFY, total fluorescence yield.

[18–29]) or maghemite (γ-Fe_2O_3 [30–37]). Miedema and de Groot [38] have recently published a comprehensive overview of Fe 2p spectroscopy of Fe oxides and other Fe compounds. These authors maintain a web site (www.anorg.chem.uu.nl/xaseels/) which provides a complete listing and links to all references reporting Fe 2p spectra. Despite the extensive studies, the published X-ray absorption spectra of magnetite are not consistent and often contradict each other. A representative sample of this literature is summarized in Table 1 where the reported spectra are categorized as falling into one of two shapes. Specifically, some of the published Fe L_3 spectra of Fe_3O_4 exhibit a low energy shoulder at ~708 eV (about 1.5 eV below the main $2p_{3/2} \rightarrow 3d$ peak), while the others do not. Similarly, some of the published Fe L_3 spectra of γ-Fe_2O_3 exhibit a low energy shoulder at ~708 eV, while the others do not. This raises the question, *what is the correct spectrum of each of these important materials?*

Here, we report a detailed investigation of the Fe L_{23} XAS of magnetite. We used scanning transmission X-ray microscopy (STXM) to measure XAS spectra of the bulk material and thus reduce the sensitivity to surface oxidation, while at the same time using the high spatial resolution of STXM (30 nm) so that particles in the few hundred nm size scale can be measured in order to avoid absorption saturation. Two representative types of magnetite were studied: one type is magnetite nanocrystals extracted from the magnetotactic bacterium (MTB), *Magnetovibrio blakemorei* strain MV-1 [39]; the other type is chemically synthesized nano-magnetite, obtained commercially from Sigma–Aldrich. A detailed comparative study of the Fe L_{23} XAS and XMCD of biogenic versus abiogenic magnetite nanoparticles was published by Carvallo et al. [40]; our results are compared to theirs. The organization of the paper is as follows. After describing materials and experimental techniques (Section 2), the existence of an extra shoulder in the low-energy side of L_3 spectrum of abiogenically produced nano-magnetite, as compared with the L_3 spectrum of biogenic magnetite, is documented (Section 3.1). Powder X-ray diffraction (Section 3.2) is used to show that the biogenic magnetite is stoichiometric Fe_3O_4 and that the abiogenic nano-magnetite is an intermediate phase between Fe_3O_4 and γ-Fe_2O_3. We then show that the extra shoulder on the low-energy side of the Fe L_3 spectrum can be "switched off" by H_2 reduction (Section 3.3) or "switched on" by air oxidization (Section 3.4). We also document that the membrane enveloping the magnetite crystals in cells of *M. blakemorei* can protect magnetite crystals from air oxidation for a surprisingly long period of time. Our results are compared to those of Carvallo et al. [40] in Section 4, followed by a summary in Section 5.

2. Experimental methods

Nano-magnetite powder (average particle size of 5 nm, stated purity of >95%) was purchased from Sigma–Aldrich [41]. The biogenic magnetite crystals were extracted from cells of *M. blakemorei* strain MV-1, which were grown anaerobically in liquid cultures with nitrous oxide as the terminal electron acceptor as previously described [42]. Cells were harvested from cultures at mid- to late-exponential phase of growth. By using the procedure described by Alphandéry et al. [43], the membrane-encased magnetite crystals, referred to as magnetosomes, were extracted from cells of MV-1. For some studies the membranes enclosing the magnetosomes were removed to accelerate oxidization by suspending extracted magnetosomes in 1% aqueous sodium dodecyl sulfate (SDS) and sonicating for 15 min at a power of 15 W. Finally, these stripped magnetosomes were heated at 600 °C in air for 3 h. The samples were imaged with a JEOL Model JEM 1200 EX transmission electron microscope. The phase composition was determined by powder X-ray diffraction (XRD) using a Bruker D8 Advance instrument with Co Kα or Cu Kα radiation.

STXM measurements were performed at the soft X-ray spectromicroscopy (SM) beamline (10ID1) at the Canadian Light Source (CLS), Saskatoon, Canada [44]. The beamline was operated at an energy resolving power $E/\Delta E > 3000$. The source point for the CLS SM beamline is an elliptically polarizing undulator (EPU) which provides nearly 100% circularly polarized light at the Fe L_{23} edge. The samples were mounted on a flat sample plate. The bottom 20% of the plate (that to which the grid sample was attached) was cut to generate a narrow strip which could be twisted by 30° about the long axis of the plate in order to achieve a 50% projection of the magnetization vector onto the direction of the incident X-ray beam. The tilt sample plate was mounted on an interferometrically controlled piezo stage, without any additional applied magnetic field. Images were measured in transmission mode by raster scanning the sample over the region of interest while detecting the transmitted signal. Spectral data was acquired by collecting a sequence of images over the energy range of interest, called a "stack" [45]. In order to measure the Fe L_3-edge XMCD, image sequences were recorded with both left circularly polarized light (LCP) and right circularly polarized light (RCP), with alternation

of the circular polarization at each photon energy. This concurrent acquisition mode [46] results in higher quality spectral data than when the full RCP and LCP spectra are recorded sequentially [47]. Data analysis was performed using aXis2000 [48]. The RCP and LCP stacks were combined and aligned together. The transmission signals were converted to optical densities using the incident flux signals through a region free of Fe but adjacent to the region under study. The acquired stacks (after alignment and conversion to optical density) consist of a near edge X-ray absorption fine structure (NEXAFS) spectrum at each pixel. The X-ray magnetic circular dichroism (XMCD) stack was obtained from the difference of the signals recorded with the two types of circular polarization. The L_3 and L_2 signals are only presented for some samples due to limited beam time to make measurements. The L_2 signal provides complementary information to the L_3 signal. However the L_2 signal is ~3 times weaker than the L_3 signal. Thus ~10 times more beam time would be needed to define the L_2 signal to the same quality as measured for the L_3 signal. Since measurement of just the L_3 edge take several hours per spectrum due to the very small amount of material being examined, it was not practical to record complete Fe L_{23} spectra in all cases, especially considering that access to the beam time on the high performance STXM beamlines needed for this work is very competitive.

3. Results

3.1. X-ray absorption spectroscopy

Fig. 1a shows the Fe L_{23} spectrum of a magnetized magnetite thin film recorded with the photon polarization parallel (red) and antiparallel (green) to the sample magnetization using total electron yield (TEY) detection [24]. That sample was very carefully prepared and is believed to be stoichiometric Fe_3O_4. Its spectrum agrees with that we measure from the biogenic MV1 magnetite [46], which supports the use of the spectra reported by Goering et al. [24] as the true spectrum of magnetite – see below. The XMCD spectrum (blue), the spectrum recorded with the photon polarization parallel minus that recorded with the photon polarization antiparallel to the sample magnetization, is also shown. The XMCD intensity of the Goering et al. [24] data has been reduced by a factor of 2 to make a valid comparison to the XMCD derived from the STXM-XAS spectra, since the magnetization of the MV-1 magnetosomes is in the plane of the sample which is tilted 30° from the normal to the X-ray beam and thus only 50% of the magnetic moment of the chain is aligned along the photon polarization vector [47]. Fe L_{23} XAS spectra exhibit two main bands which are the L_3 ($2p_{3/2}$) and L_2 ($2p_{1/2}$) peaks separated by the spin-orbit coupling of the 2p hole. Each band has a fine structure which is determined by a complex interplay of ligand field splitting, covalent interactions and atomic multiplets for each of the three distinct electronic/magnetic sites in magnetite [18,49,50]. Fig. 1b presents the Fe L_{23} spectra and XMCD of a chain of magnetite magnetosomes inside a single cell of the magnetotactic bacterium *M. blakemorei* strain MV-1, recorded using transmission detection in STXM [46]. The inset indicates the magnetosome chain from which the spectra were obtained. Fig. 1c shows the Fe L_{23} spectrum and XMCD of the as-received Sigma–Aldrich nano-magnetite powder. The inset is a STXM optical density image of the aggregate of Sigma–Aldrich nano-magnetite particles from which the XAS signals were extracted. In contrast to the spectra reported by Goering et al. [24] or the spectra of the magnetosomes [46], the L_3 spectrum of the abiogenic nano-magnetite exhibits an additional peak at 708 eV, which was not observed in biogenic magnetite synthesized by magnetotactic bacteria [46,47]. We note that the XAS spectrum of nano-magnetite presented in Fig. 1c matches well with

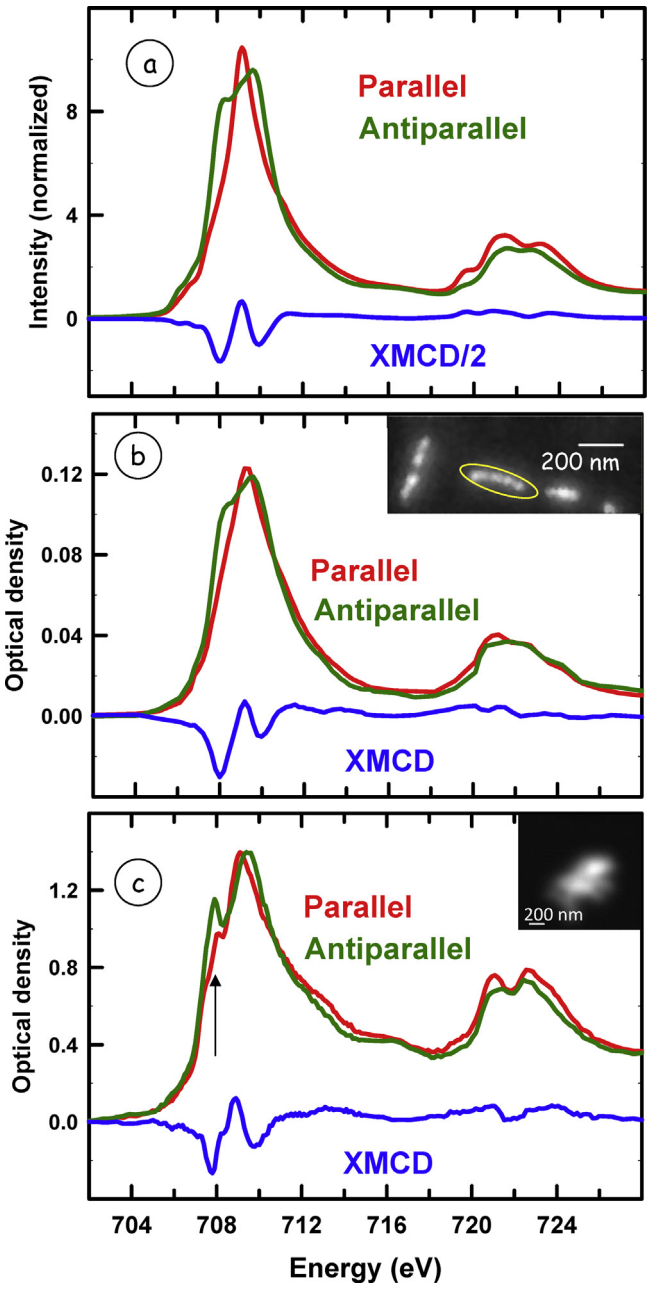

Fig. 1. (a) Fe L_{23} X-ray absorption (XAS) spectra of thin film magnetite recorded using total electron yield detection, with circularly polarized X-rays parallel (red) and antiparallel (green) with respect to the sample magnetization (data courtesy of Goering et al. [24]). A polynomial was fit to the pre-edge signal and the intensity at 730 eV was unit-normalized. The difference signal (parallel minus antiparallel), the X-ray magnetic circular dichroism (XMCD, blue) is plotted using the same vertical scaling. The XMCD in (a) is divided by two, as the XMCD measured in the STXM is only ½ of the full amount due to use of a 30° sample tilt angle [47]. (b) Fe L_{23} spectra of a chain of magnetite magnetosomes from *Magnetovibrio blakemorei* strain MV-1, recorded in STXM with circularly polarized X-rays parallel (red) and antiparallel (green) to the magnetization of the sample. The inset is a STXM image of the magnetosomes from which the spectra were obtained. (c) Fe L_{23} XAS spectra of the as-received Sigma–Aldrich nano-magnetite powder recorded in STXM with circularly polarized X-rays parallel (red) and antiparallel (green) to the magnetization of the sample. The inset is a STXM optical density image of the agglomerate of nano-magnetite particles from which the XAS signals were extracted. In each case, the XMCD spectrum (blue), the difference signal (parallel minus antiparallel), is shown below the spectral curves. (For interpretation of the references to color in this figure legend, the reader is referred to the web version of this article.)

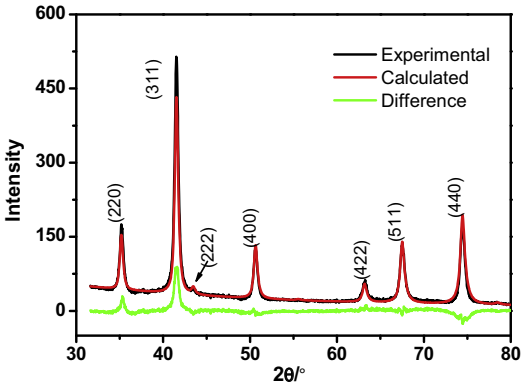

Fig. 2. XRD powder pattern of nano-magnetite as-received from Sigma–Aldrich, recorded using Co Kα radiation. The experimental (black) and calculated (red) powder patterns (for magnetite, but with modified unit cell parameters, as discussed in the text) are plotted, along with the difference (experimental minus calculated patterns) (green). The peaks are labeled with their corresponding crystallographic planes. (For interpretation of the references to color in this figure legend, the reader is referred to the web version of this article.)

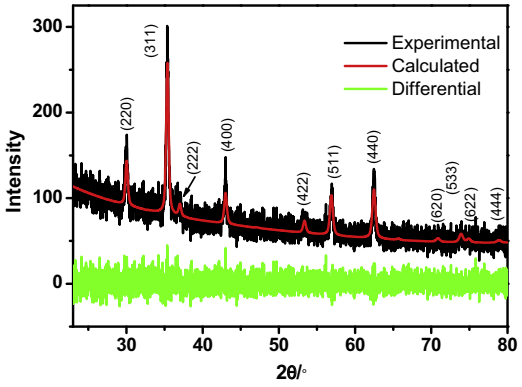

Fig. 3. XRD powder pattern of nano-magnetite reduced with H_2. For technical reasons, this signal was recorded using Cu Kα radiation, which resulted in a larger noise level due to Fe Kα fluorescence, which is excited by the Cu Kα but not the Co Kα line. The experimental (black) and calculated (red) powder patterns (for magnetite, with unit cell parameters similar to that for magnetite, as discussed in the text) are plotted, along with the difference (experimental minus calculated patterns) (green). The peaks are labeled with their corresponding crystallographic planes. (For interpretation of the references to color in this figure legend, the reader is referred to the web version of this article.)

that which has been reported for maghemite by several groups, such as that reported by Kim et al. [33].

Total electron yield (TEY) is a common detection mode used to measure X-ray absorption spectra. Nolle et al. [51] applied both TEY and transmission mode detection to measure XAS and XMCD spectra of $FePt/FeO_x$. They observed a higher oxidation state at the surface of the sample when the detection mode was switched from transmission to TEY. The Fe L_{23} spectra of biogenic magnetite synthesized extracellularly by *Shewanella oneidensis* MR-1 were found to exhibit the lower energy 708 eV shoulder in the L_3 region when TEY detection mode was used [52] but not when transmission detection was used (see Fig. 3 in Ref. [53]). Likewise, Peak et al. [54] observed the 708 eV shoulder in Fe L_3 spectra of synthetic magnetite when TEY detection mode was employed. TEY is highly surface sensitive and heavily influenced by surface oxidation. Previous studies have shown that brief exposure (<1 day) of Fe_3O_4 films to the atmosphere does not affect the XAS and XMCD measurements, whereas longer exposures would oxidize the surface of the films [18,55]. This could explain the lower energy shoulder in the L_3 region that is often, but not always – see Table 1, observed with TEY detection. In the present work transmission detection in STXM was used, which is more bulk sensitive and less likely to be affected by surface oxidation. Thus, our spectra, measured in transmission mode, are more likely to reflect the intrinsic spectrum of a sample than TEY mode measurements on the same sample. It should be noted that the STXM samples need to be quite small to avoid absorption saturation. The magnetosomes examined in this work are typically 50 nm in diameter, while the nano-magnetite samples are in the range of 20–30 nm. At this size scale the particle surface is still an insignificant fraction of the total sample. At 50 nm diameter, assuming a surface modification over ~1 nm at the surface, the surface contribution would be of the order of 10^{-4}. However, for nanoparticle samples with diameters below 5 nm where a 1 nm zone at the surface contains about 10% of the material, the differences between transmission and TEY detection would be minimal.

3.2. Powder diffraction

Fig. 2 presents powder X-ray diffraction (XRD) patterns of the as-received Sigma–Aldrich nano-magnetite sample. The peaks are labeled according to their crystallographic planes. Although the XRD patterns of nano-magnetite and nano-maghemite are nearly identical due to their structural similarities, the unit-cell length obtained from the XRD can be used to distinguish these two oxides [14]. The unit-cell length of the Sigma–Aldrich nano-magnetite was determined to be 8.3638± 0.0004 Å ($a = b = c$) using the Rietveld method. This value lies between the cell length of pure magnetite (8.3941 Å) and that of pure maghemite (8.3474 Å). This suggests that the as-received Sigma–Aldrich nano-magnetite sample was not pure magnetite, but rather a nonstoichiometric magnetite, an intermediate phase between magnetite and maghemite. The ratio of Fe(II) to Fe(III) oxidation states can be determined by an equation developed by Gorski and Scherer [14]:

$$a = 0.1094x_d + 8.3424 \quad (1)$$

where a is the unit-cell length and x_d is the ratio of the amount of total Fe(II) in the octahedral sites to that of total Fe(III) in both octahedral and tetrahedral sites. Based on this equation the Fe(II)/Fe(III) ratio in the as-received Sigma–Aldrich nano-magnetite sample was 0.2, which is considerably smaller than the value of 0.5 for pure magnetite. Oxidation of magnetite (Fe_3O_4) to maghemite (Fe_2O_3) causes the Fe(II)/Fe(III) ratio to decrease. If magnetite was completely oxidized to maghemite, the Fe(II)/Fe(III) ratio would be 0. Thus, the powder diffraction data suggests that almost half of the total Fe(II) ions in as-received Sigma–Aldrich nano-magnetite had been oxidized to Fe(III). In other words, the Sigma–Aldrich nano-magnetite was actually partially oxidized magnetite, or an intermediate phase between magnetite and maghemite. *Is the additional peak observed at 708 eV in the Fe-L_3 XAS of Sigma–Aldrich nano-magnetite related to this partial oxidization*?

3.3. Generating pure magnetite from the commercial sample

To investigate this hypothesis, the as-received Sigma–Aldrich nano-magnetite powder was heated under a H_2 atmosphere at 309 °C for 0.5 h. Fig. 3 shows the XRD pattern of a Sigma–Aldrich nano-magnetite sample after reduction by H_2. The data is significantly noisier than that in Fig. 2 due to Fe Kα fluorescence background since Cu Kα rather than Co Kα radiation was used. The peaks are labeled with their corresponding crystallographic planes. The unit-cell length of H_2-reduced Sigma–Aldrich nano-magnetite, extracted by the Rietveld method, was 8.4058 ± 0.0007 Å. This value is in a good agreement with the reported unit-cell length of pure magnetite (8.3941 Å) [9], indicating that the previously partial oxidized Sigma–Aldrich nano-magnetite had been successfully reduced to pure magnetite.

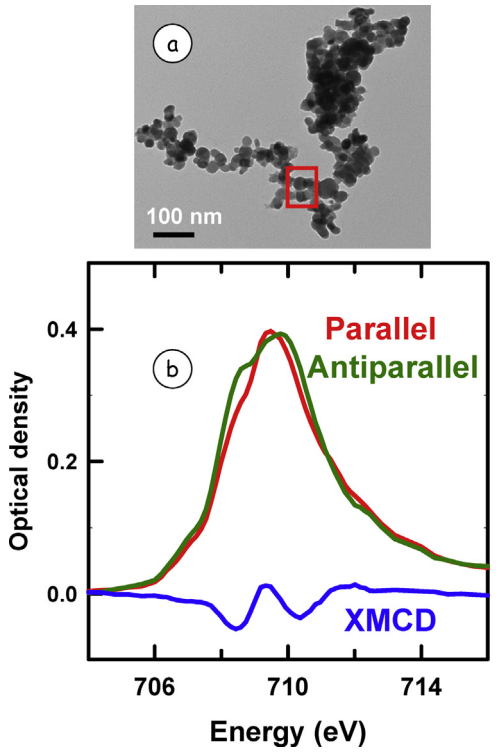

Fig. 4. (a) TEM image of H_2-reduced Sigma–Aldrich nano-magnetite powder. The red square indicates the area from which the Fe L_{23} XAS spectra were extracted. (b) Fe L_{23} XAS and XMCD spectra of the H_2-reduced Sigma–Aldrich nano-magnetite powder recorded with circularly polarized X-rays parallel (red) and antiparallel (green) to the magnetization of the sample. (For interpretation of the references to color in this figure legend, the reader is referred to the web version of this article.)

Fig. 4a is a transmission electron microscopy (TEM) image of H_2-reduced Sigma–Aldrich nano-magnetite powder. The Fe L_{23} XAS spectrum was measured from the area in the red square. Fig. 4b shows the Fe L_{23} XAS spectra of the H_2-reduced Sigma–Aldrich nano-magnetite powder recorded using X-rays with parallel (red) and antiparallel (green) polarization relative to the sample magnetization, along with the derived XMCD (blue). Fig. 4b shows that the peak previously observed at 708 eV in the Fe L_{23} XAS spectrum of the as-received Sigma–Aldrich nano-magnetite (Fig. 1c) was eliminated by H_2 reduction. Thus, the additional peak at 708 eV in the Fe L_{23} XAS spectra of as-received Sigma–Aldrich nano-magnetite is caused by partial oxidization. Thus we assume that similar peaks observed in the Fe L_3-edge XAS of Fe_3O_4 reported by Garcia et al. [21] and Pool et al. [26] (among others) are also due to partial oxidation, either at the surface, and sensed preferentially due to the TEY detection, or from the bulk, due to a non-stoichiometric synthesis or the overall sample being partially oxidized.

3.4. Generating oxidized magnetite from magnetosomes

Fig. 5a presents a TEM image of a biogenic magnetite chain extracted from a cell of *M. blakemorei* (MV-1). Fig. 5b shows the Fe L_3 XAS spectra of biogenic magnetite magnetosomes extracted from cells of *M. blakemorei* (Fig. 5a). The parallel (red), antiparallel (green) spectra and the XMCD (blue) all appear similar to the spectra of intracellular magnetosomes in cells of *M. blakemorei* (Fig. 1b) [46,47], and the spectra of H_2-reduced Sigma–Aldrich nano-magnetite (Fig. 4b). X-ray diffraction determined the unit-cell length of these extracted biogenic magnetite crystals to be 8.402 Å, indicating that magnetite crystals biomineralized by magnetotactic bacteria are stoichiometric, as determined and reported

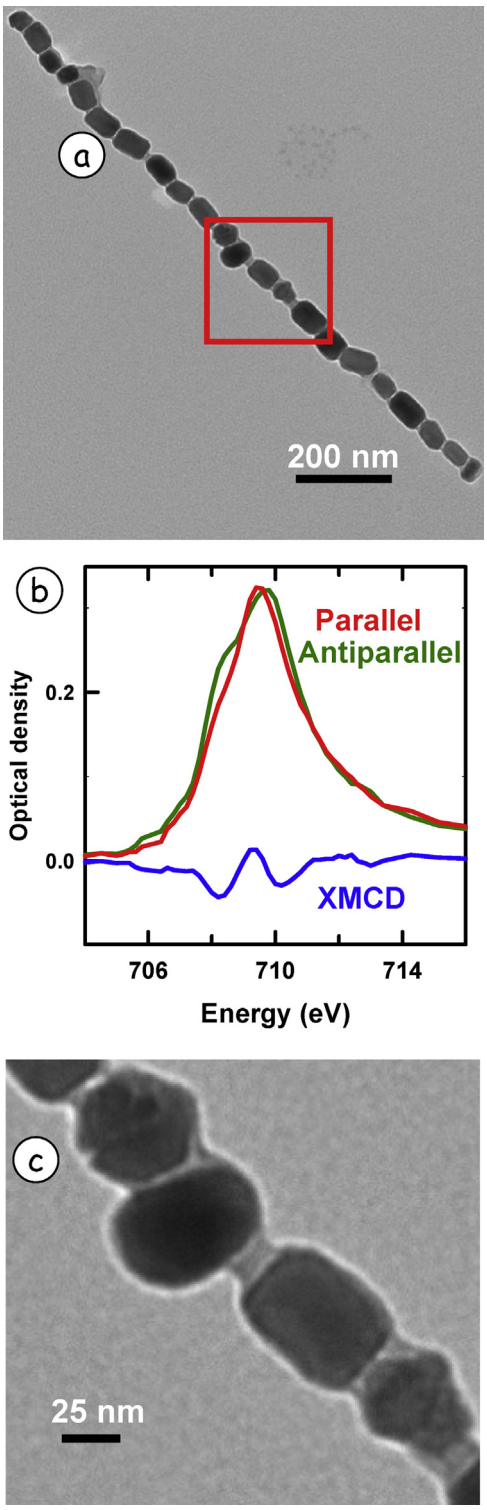

Fig. 5. (a) TEM image of the biogenic magnetite chain extracted from cells of the magnetotactic bacterium *Magnetovibrio blakemorei* strain MV-1. (b) Fe L_3 XAS spectra and XMCD of the biogenic magnetite chain extracted from MV-1 recorded with circularly polarized X-rays parallel (red) and antiparallel (green) to the magnetization of the sample. (c) Magnified TEM image corresponding to the red area labeled in (a). (For interpretation of the references to color in this figure legend, the reader is referred to the web version of this article.)

elsewhere [56]. Careful comparison of the magnitude of the XMCD signal from intact MV-1 cells with that from the Goering et al. [24] data has shown that intracellular magnetosomes are fully magnetized [46]. Thus, the Fe L_{23} XAS and XMCD spectra measured from

biogenic magnetite can be considered as the standard spectrum of magnetite.

The extracted magnetosome chain sample experienced significant air contact between the time it was extracted and the time it was measured, yet there is little or no evidence of oxidation. *Why are the long time air-exposed extracted biogenic magnetosomes still stoichiometric?* Note that transmission X-ray detection was used for the spectra reported in both Figs. 4 and 5 and thus they are characteristic of the bulk of the sample, not the surface. Fig. 5c shows a magnified TEM image corresponding to the red area labeled in Fig. 5a. A dense membrane tightly adhering to these magnetite crystals is observed. This membrane may limit air contact, thereby effectively protecting the magnetic crystals from being oxidized.

In order to probe the protective character of the membrane, the biogenic magnetite extracted from cells of a magnetotactic bacterium, *M. blakemorei* strain MV-1, was investigated after prolonged oxidation. Fig. 6a–c present Fe L_3 spectra of magnetosome chains extracted from *M. blakemorei* recorded over an extended time period. These magnetosome chains were enclosed by membranes, as shown in the inset in each panel, and were exposed to air for 1 week, 2 months, and 8 months, respectively. As shown in Fig. 6c, the magnetosome chain which was exposed to air for 8 months still does not exhibit any extra peak on the low energy side of the Fe L_3-edge XAS spectra, but rather its spectrum is similar to the magnetosome chain exposed in air for only one week (Fig. 6a). This indicates that the membrane enclosing the magnetosomes effectively protects the magnetite single crystals from oxidation by air for a relatively long time. In order to further quantify the proportional changes of Fe ions in these stripped magnetosome chains, we compare the three XMCD spectra obtained from stripped magnetosome chains with the one acquired from the intracellular magnetosome chain, and with the reference XMCD spectrum reported by Goering et al. [24] (see Fig. 6d). All the XMCD spectra in Fig. 6d are similar, indicating that the membrane allows these extracted magnetosome chains to effectively resist air oxidization under ambient conditions. The excellent match in the XMCD intensity (after correction for the 50% reduction due to the 30° tilt geometry we use) between all of the magnetosome signals (which are measured without an externally applied field) with that from a magnetite thin film in a strong external magnetic field [24] shows that both the intracellular magnetosomes [46] and the stripped magnetosomes are highly stoichiometric, and are fully magnetized.

Gao et al. [57] reported that Fe_3O_4 nanoparticles are partly transformed into γ-Fe_2O_3 after heating at 200 °C for 3 h in air and are completely transformed into γ-Fe_2O_3 if they are heated at 600 °C for 3 h. In order to investigate the corresponding transformation for biogenic magnetite, we took biogenic magnetite isolated from MV-1 bacteria, stripped it of its membrane with surfactant, and heated it in air at 600 °C for 3 h. Fig. 7a presents a TEM image while Fig. 7b shows the Fe L_3 XAS spectra of the air-heated biogenic magnetite crystals recorded with parallel (red) and antiparallel (green) polarization, and the associated XMCD (blue). A strong peak is observed at 708 eV (labeled by an arrow in Fig. 7b). This is similar to the structure observed at the low energy side of the Fe L_3-edge signal of as-received Sigma–Aldrich nano-magnetite (Fig. 1c). This supports our interpretation that the Sigma–Aldrich nano-magnetite was a partially oxidized phase. Also, the experimental results for oxidized magnetosomes match well with a theoretical prediction that the Fe L_{23}XAS of maghemite should exhibit a peak on the lower energy side of the L_3 peak [58]. Finally, we suspect the reason that Fe L_{23} XAS spectra of maghemite reported by Anders et al. [30] and Brice-Profeta et al. [32] did not exhibit a peak on the lower energy side of the L_3 peak was due to the fact that their supposed maghemite samples were not pure maghemite but rather a mixture with a large fraction of magnetite.

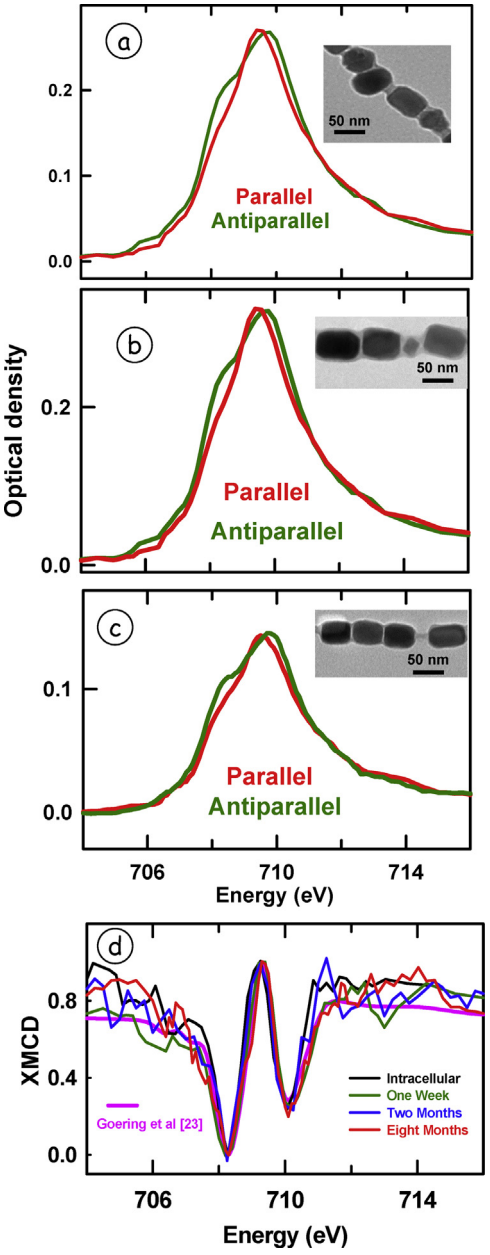

Fig. 6. Fe L_3 spectra of the extracted magnetosome chains, which have been exposed in air for (a) 1 week, (b) 2 months, and (c) 8 months, recorded with circularly polarized X-rays parallel (red) and antiparallel (green) to the magnetization of the sample. The insets in (a)–(c) indicate the magnetosome chains enclosed by the magnetosome membrane from which these spectra were obtained. (d) Comparison of the XMCD spectra, the difference signal (parallel minus antiparallel), for all three samples of the extracted magnetosome chains (1 week (green), 2 months (blue), 8 months (red)) and that of the intracellular magnetosome chain (black). The XMCD reported by Goering et al. [24] is also plotted, scaled by 50% (pink). (For interpretation of the references to color in this figure legend, the reader is referred to the web version of this article.)

4. Discussion

Carvallo et al. [40] presented a detailed study of the Fe L_{23} XAS and XMCD of biogenic magnetite (from *Shewanella putrefaciens* CIP 59.28) and abiogenic magnetite (nanoparticles prepared by adding 1 M NaOH to a suspension of lepidocrocite in an aqueous solution of $FeCl_2$). In that work the Fe L_{23} XAS spectra are very similar to each other and to the spectra of magnetosomes from MV-1 presented here, as well as to the spectra of abiogenic magnetite reported by Goering et al. [24]. (Note that the energy scale of the Carvallo et al.

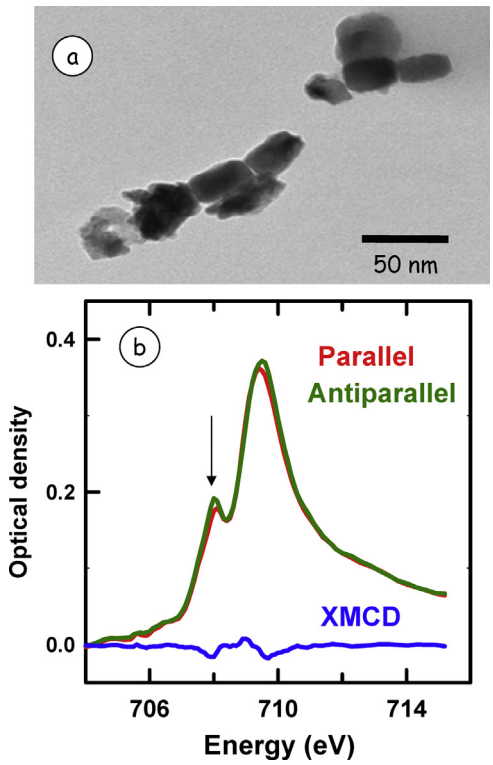

Fig. 7. (a) TEM image of the MV-1 derived magnetite heated in air at 600 C for 3 h. (b) Fe L_3 spectra of the air-heated magnetite recorded with circularly polarized X-rays parallel (red) and antiparallel (green) to the magnetization of the sample, and the associated XMCD. (For interpretation of the references to color in this figure legend, the reader is referred to the web version of this article.)

[40] spectra is displaced by almost 4 eV to higher energy – i.e. they claim the energy of the strongest XMCD signal is 712 eV, whereas our work, as well as that of Goering et al. [24] and many others, places the strongest XMCD signal at 708.2 eV.) Carvallo et al. [40] do see a small but reproducible difference in the XMCD spectra of their biogenic and abiogenic magnetite nanoparticles. By modeling the Fe L_3 XMCD signal with a linear combination of three Fe ion contributions in Fe_3O_4, they concluded that their (extracellular) biogenic nano-magnetite contained a higher amount of octahedral Fe(II) than their abiogenic nano-magnetite. In our study, we also observed differences in the XAS spectra between Sigma–Aldrich nano-magnetite and biogenic magnetite crystals biomineralized by cells of the magnetotactic bacterium *M. blakemorei*. Compared with the subtle XMCD difference investigated by Carvallo et al. [40], the difference between the XAS of biogenic and abiogenic magnetite reported in this work (Fig. 1a–c) is much larger. Based on the structural data obtained via XRD measurements (Section 3.2), it is clear that the difference between the XAS of biogenic and abiogenic magnetite found in this study is due to non-stoichiometry or partial oxidization in those samples showing the low energy L_3 peak. More importantly, we have shown that this XAS difference, the extra peak in the low energy side of L_3 region, could be "switched on" and "switched off" by using air oxidization and H_2 reduction methods, respectively. The small difference in XMCD reported by Carvallo et al. [40] may exist in our data set, but it is masked by the much larger difference due to a gross difference in the chemical nature of the two samples. Pattrick et al. [49] and Coker et al. [52] have used changes in the XMCD signal to study non-stoichiometric effects in bio-generated magnetite in a similar manner. While these results are completely credible, they are a more subtle effect than the effects reported in this work.

5. Summary

This work aimed at better understanding the reasons for inconsistencies in the literature regarding the shape of Fe L_3 XAS spectra claimed to be that of Fe_3O_4. We used STXM, powder X-ray diffraction and chemical modification to show that magnetosomes extracted from MV-1 are stoichiometric magnetite while as-received synthetic nano-magnetite was partly oxidized, with a powder pattern closer to that of γ-Fe_2O_3 than that of Fe_3O_4. Our results suggest that one of the reasons for differing literature XAS spectra of Fe_3O_4 and γ-Fe_2O_3 is due to differences in the samples. In particular, some samples that were considered to be either Fe_3O_4 or γ-Fe_2O_3 were most likely solid solutions of Fe_3O_4 and γ-Fe_2O_3. Other factors that can play a role are (i) differences in detection method, with surface-sensitive TEY being more likely to show the 708 eV feature characteristic of partial oxidation; and (ii) non-stoichiometry of Fe_3O_4 samples, in terms of modified site occupancies. X-ray absorption spectroscopy, using both the Fe L-edge spectral shape and detailed analysis of the XMCD, is a useful tool to probe site occupancies, as outlined in this work and exploited in detailed studies by Pattrick et al. [49] and Coker et al. [52]. Finally, we showed that the membrane enclosing the magnetite crystals in MV-1 magnetotactic bacteria can effectively protect magnetite crystals from being oxidized. At this point we are puzzled as to why the membrane in magnetosome extracts appears to be air-impervious, while that same membrane, inside the cell, is able to transport Fe ions and oxygen during magnetosome synthesis. Further studies are required to understand this phenomenon.

Acknowledgements

Research funded by NSERC (Canada) and the Canada Research Chairs program. X-ray diffraction was measured at the MAX crystallography facility at McMaster. STXM measurements were performed at beamline 10ID1 at the CLS, which is supported by NSERC, CIHR, NRC, the Province of Saskatchewan, WEDC, and the University of Saskatchewan. Some results were also obtained at the STXM on BL 11.0.2 at the ALS, which is supported by the Director, Office of Energy Research, Office of Basic Energy Sciences, Materials Sciences Division of the U.S. Department of Energy, under Contract No. DE-AC02-05CH11231. D.A.B. is supported by US National Science Foundation (NSF) Grant EAR-0920718 and by subcontract SC-12-384 from US Department of Energy contract DE-AC02-07CH11358 to the Ames Laboratory at Iowa State University.

References

[1] H.I. Adegoke, F.A. Adekola, O.S. Fatoki, B.J. Ximba, Pol. J. Environ. Stud. 22 (2013) 7.
[2] R.M. Cornell, U. Schwertmann, The Iron Oxides: Structures, Properties, Reactions, Occurrences and Uses, Wiley VCH Press, Weinheim, Germany, 2003.
[3] R. Zboril, A. Bakandritsos, M. Mashlan, V. Tzitzios, P. Dallas, Ch. Trapalis, D. Petridis, Nanotechnology 19 (2008) 095602.
[4] M. Mohapatra, S. Anand, Int. J. Eng. Sci. Technol. 2 (2010) 127.
[5] K. Yamaguchi, K. Matsumoto, T. Fujii, J. Appl. Phys. 67 (1990) 4493.
[6] G. Neri, A. Bonavita, G. Rizzo, S. Galvagno, S. Capone, P. Siciliano, Sens. Actuators B: Chem. 114 (2006) 687.
[7] J. Zhang, Y. Wang, H. Ji, Y. Wei, N. Wu, B. Zuo, Q. Wang, J. Catal. 229 (2005) 114.
[8] Y. Shi, M. Shi, Y. Qiao, J. Tu, H. Chen, Nanotechnology 23 (2012) 395601.
[9] M. Fleet, Acta Crystallogr. B 37 (1981) 917.
[10] M. Descostes, F. Mercier, N. Thromat, C. Beaucaire, M. Gautier-Soyer, Appl. Surf. Sci. 165 (2000) 288.
[11] J. Jolivet, P. Belleville, E. Tronc, J. Livage, Clays Clay Miner. 40 (1992) 531.
[12] E. Schmidbauer, M. Keller, J. Magn. Magn. Mater. 297 (2006) 107.
[13] G. Da Costa, E. De Grave, P. De Bakker, R. Vandenberghe, Clays Clay Miner. 43 (1995) 656.
[14] C.A. Gorski, M.M. Scherer, Am. Mineral. 95 (2010) 1017.
[15] F. De Groot, J. Fuggle, B. Thole, G. Sawatzky, Phys. Rev. B 42 (1990) 5459.
[16] C. Chen, Y. Idzerda, H.-J. Lin, N. Smith, G. Meigs, E. Chaban, G. Ho, E. Pellegrin, F. Sette, Phys. Rev. Lett. 75 (1995) 152.

[17] A.P. Hitchcock, Soft X-ray imaging and spectromicroscopy, in: G.V. Tendeloo, D.V. Dyck, S.J. Pennycook (Eds.), Handbook of Nanospectroscopy, Wiley VCH Press, Weinheim, Germany, 2012, p. 745.
[18] P. Kuiper, B.G. Searle, L.-C. Duda, R.M. Wolf, P.J. van der Zaag, J. Electron Spectrosc. Relat. Phenom. 86 (1997) 107.
[19] F. Schedin, P. Morrall, V. Petrov, S. Case, M. Thomas, E. Dudzik, G. Van der Laan, G. Thornton, J. Magn. Magn. Mater. 211 (2000) 266.
[20] A. De Castro, P. Fonseca, J. Pacheco, J. Da Silva, E. Da Silva, M. Santana, J. Magn. Magn. Mater. 233 (2001) 69.
[21] J. García, G. Subías, J. Phys.: Condens. Matter 16 (2004) R145.
[22] Y. Lee, J. Lee, C.J. Bae, J.G. Park, H.J. Noh, J.H. Park, T. Hyeon, Adv. Funct. Mater. 15 (2005) 503.
[23] P. Thakur, W.K. Choi, K.H. Chae, J. Korean Phys. Soc. 53 (2008) 3694.
[24] E.J. Goering, M. Lafkioti, S. Gold, G. Schuetz, J. Magn. Magn. Mater. 310 (2007) e249.
[25] E. Goering, Phys. Status Solidi B 248 (2011) 2345.
[26] V. Pool, M. Klem, C. Chorney, E. Arenholz, Y. Idzerda, J. Appl. Phys. 109 (2011) 07B529.
[27] A. Michelin, E. Drouet, E. Foy, J. Dynes, D. Neff, P. Dillmann, J. Anal. At. Spectrom. 28 (2013) 59.
[28] Z. Wang, L. Wu, J. Zhou, W. Cai, B. Shen, Z. Jiang, J. Phys. Chem. C 117 (2013) 5446.
[29] P.J. Wong, W. Zhang, K. Wang, G. van der Laan, Y. Xu, W.G. van der Wiel, M.P. de Jong, J. Mater. Chem. C 1 (2013) 1197.
[30] S. Anders, M. Toney, T. Thomson, R. Farrow, J.-U. Thiele, B. Terris, S. Sun, C. Murray, J. Appl. Phys. 93 (2003) 6299.
[31] S. Sun, H. Zeng, D.B. Robinson, S. Raoux, P.M. Rice, S.X. Wang, G. Li, J. Am. Chem. Soc. 126 (2004) 273.
[32] S. Brice-Profeta, M. Arrio, E. Tronc, I. Letard, C.C. dit Moulin, P. Sainctavit, Phys. Scr. T 115 (2005) 626.
[33] D. Kim, H. Lee, G. Kim, Y. Koo, J. Jung, H. Shin, J.-Y. Kim, J.-S. Kang, Phys. Rev. B 79 (2009) 033402.
[34] B. Gilbert, J.E. Katz, J.D. Denlinger, Y. Yin, R. Falcone, G.A. Waychunas, J. Phys. Chem. C 114 (2010) 21994.
[35] R. Desautels, E. Skoropata, Y. Chen, H. Ouyang, J. Freeland, J. van Lierop, J. Phys.: Condens. Matter 24 (2012) 146001.
[36] E. Lee, D. Kim, J. Hwang, K. Lee, S. Yoon, B. Suh, K.H. Kim, J.-Y. Kim, Z. Jang, B. Kim, Appl. Phys. Lett. 102 (2013) 133703.
[37] C. Piquer, M.A. Laguna-Marco, A.G. Roca, R. Boada, C. Guglieri, J. Chaboy, J. Phys. Chem. C 118 (2014) 1332.
[38] P.S. Miedema, F.M.F. de Groot, J. Electron Spectrosc. Relat. Phenom. 187 (2013) 32.
[39] D.A. Bazylinski, T.J. Williams, C.T. Lefèvre, D. Trubitsyn, J. Fang, T.J. Beveridge, B.M. Moskowitz, B. Ward, S. Schübbe, B.L. Dubbels, Int. J. Syst. Evol. Microbiol. 63 (2013) 1824.
[40] C. Carvallo, P. Sainctavit, M.-A. Arrio, N. Menguy, Y. Wang, G. Ona-Nguema, S. Brice-Profeta, Am. Mineral. 93 (2008) 880.
[41] CAS Number: 1317-61-9; Assay: 95%; Particle Size: <5 μm (accessed January 2014).
[42] A.J. Dean, D.A. Bazylinski, Curr. Microbiol. 39 (1999) 219.
[43] E. Alphandéry, Y. Ding, A. Ngo, Z. Wang, L. Wu, M. Pileni, ACS Nano 3 (2009) 1539.
[44] K. Kaznatcheev, C. Karunakaran, U. Lanke, S. Urquhart, M. Obst, A. Hitchcock, Nucl. Instrum. Methods B 582 (2007) 96.
[45] C. Jacobsen, S. Wirick, G. Flynn, C. Zimba, J. Microsc. 197 (2000) 173.
[46] S.S. Kalirai, K.P. Lam, D.A. Bazylinski, U. Lins, A.P. Hitchcock, Chem. Geol. 300 (2012) 14.
[47] K.P. Lam, A.P. Hitchcock, M. Obst, J.R. Lawrence, G.D. Swerhone, G.G. Leppard, T. Tyliszczak, C. Karunakaran, J. Wang, K. Kaznatcheev, Chem. Geol. 270 (2010) 110.
[48] A.P. Hitchcock, aXis2000 is Written in Interactive Data Language (IDL), 2014, It is available free for non-commercial use from: http://unicorn.mcmaster.ca/aXis2000.html
[49] R.A. Pattrick, G. Van Der Laan, C.M.B. Henderson, P. Kuiper, E. Dudzik, D.J. Vaughan, Eur. J. Mineral. 14 (2002) 1095.
[50] V.N. Antonov, B.N. Harmon, A.N. Yaresko, Phys. Rev. B 67 (2003) 024417.
[51] D. Nolle, E. Goering, T. Tietze, G. Schütz, A. Figuerola, L. Manna, New J. Phys. 11 (2009) 033034.
[52] V.S. Coker, C.I. Pearce, C. Lang, G. van der Laan, R.A. Pattrick, N.D. Telling, D. Schüler, E. Arenholz, J.R. Lloyd, Eur. J. Mineral. 19 (2007) 707.
[53] V. Coker, J. Byrne, N. Telling, G. Van der Laan, J. Lloyd, A. Hitchcock, J. Wang, R. Pattrick, Geobiology 10 (2012) 347.
[54] D. Peak, T. Regier, Environ. Sci. Technol. 46 (2012) 3163.
[55] F. Schedin, E. Hill, G. Van der Laan, G. Thornton, J. Appl. Phys. 96 (2004) 1165.
[56] J. Li, Y. Pan, Geomicrobiol. J. 29 (2012) 362.
[57] M. Gao, W. Li, J. Dong, Z. Zhang, B. Yang, World J. Condens. Matter Phys. 1 (2011) 49.
[58] J. Crocombette, M. Pollak, F. Jollet, N. Thromat, M. Gautier-Soyer, Phys. Rev. B 52 (1995) 3143.

Further reading

[59] A.J.M. Kuipers, V.A.M. Brabers, Phys. Rev. B 14 (1976) 1401.